

Review

# SrTiO<sub>3</sub>—Glimpses of an Inexhaustible Source of Novel Solid State Phenomena

Wolfgang Kleemann <sup>1,\*</sup>, Jan Dec <sup>2</sup>, Alexander Tkach <sup>3</sup> and Paula M. Vilarinho <sup>3</sup>

<sup>1</sup> Applied Physics, University Duisburg-Essen, D-47048 Duisburg, Germany

<sup>2</sup> Institute of Physics, University of Silesia, PL-40-007 Katowice, Poland; jan.dec@us.edu.pl

<sup>3</sup> Department of Materials and Ceramic Engineering, CICECO—Aveiro Institute of Materials, University of Aveiro, P-3810-193 Aveiro, Portugal; atkach@ua.pt (A.T.); paula.vilarinho@ua.pt (P.M.V.)

\* Correspondence: wolfgang.kleemann@uni-due.de; Tel.: +49-1575-226-3908

Received: 6 August 2020; Accepted: 30 September 2020; Published: 4 October 2020

**Abstract:** The purpose of this selective review is primarily to demonstrate the large versatility of the insulating quantum paraelectric perovskite SrTiO<sub>3</sub> explained in “Introduction” part, and “Routes of SrTiO<sub>3</sub> toward ferroelectricity and other collective states” part. Apart from ferroelectricity under various boundary conditions, it exhibits regular electronic and superconductivity via doping or external fields and is capable of displaying diverse coupled states. “Magnetoelectric multiglass (Sr,Mn)TiO<sub>3</sub>” part, deals with mesoscopic physics of the solid solution SrTiO<sub>3</sub>:Mn<sup>2+</sup>. It is at the origin of both polar and spin cluster glass forming and is altogether a novel multiferroic system. Independent transitions at different glass temperatures, power law dynamic criticality, divergent third-order susceptibilities, and higher order magneto-electric interactions are convincing fingerprints.

**Keywords:** strontium titanate; quantum paraelectricity; quantum fluctuations; ferroelectricity; isotope exchange; external stress; polar metal; superconductivity; phase coexistence; magnetoelectric multiglass.

## 1. Introduction

In this review, we focus onto two research lines of strontium titanate, SrTiO<sub>3</sub> (STO):

(1) the low-temperature phases around the quantum critical point of pure STO, and (2) the disordered electric and magnetic dipolar glassy phases in the solid solution STO: Mn. It is not intended to describe the full extent of all phenomena observed and to detail all of their properties from abundantly issued publications. We merely try to give an impression of some actual fields, which are partially related to our earlier cooperation with K. A. Müller and J. G. Bednorz.

STO is probably the most versatile perovskite-type oxide and one of the richest materials in terms of functionalities. In 1979, Müller and Burkard [1] reported that the planar permittivity of STO strongly increased upon cooling from  $\approx 300$  at room temperature and saturated with  $\epsilon'_{<110>} \approx 2.5 \cdot 10^4$  as  $T \rightarrow 0$  (comparable to  $\epsilon'_{<100>}$  vs.  $T$ , cf. Figure 1, curve 1 [2]). They conjectured a “quantum paraelectric” ground state in close proximity to a ferroelectric (FE) one, where the centrosymmetric tetragonal lattice structure of STO becomes stabilized by quantum fluctuations of the nearly softening in-plane  $F_{1u}$  lattice mode.

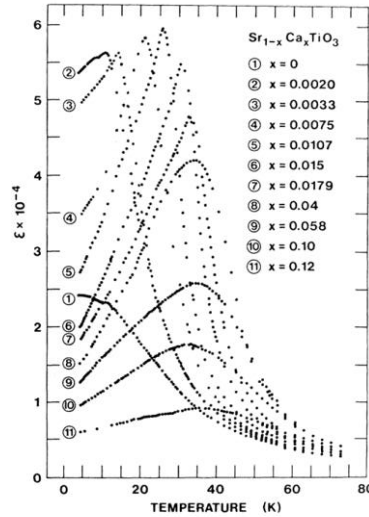


**Figure 1.** Temperature dependence of the dielectric permittivity  $\epsilon'_{[100]}$  of  $\text{Sr}_{1-x}\text{Ca}_x\text{TiO}_3$  crystals with  $0 \leq x \leq 0.12$  [2].

Quantum corrections to the temperature were proposed to describe the critical behavior of STO from the beginning [1]. In order to account for the obvious deviations from the mean-field Curie–Weiss behavior, some of us proposed a generalized modified “quantum Curie–Weiss law” [3].

$$\epsilon' = C / (T^Q - T_0^Q)^\gamma \quad (1)$$

where  $C$  stands for the Curie constant,  $\gamma$  for the critical exponent, and  $T_0^Q = T_S \coth(T_S/T_0)$  for the quantum critical temperature with classic critical temperature  $T_0$  and saturation temperature  $T_S$  being related to the ground state energy of the quantum oscillator,  $E_0 = k_B T_S$ . Crucial novel ingredients are the free parameter  $\gamma$  and the quantum temperature scale,  $T^Q = T_S \coth(T_S/T)$ , which replaces  $T$ . The best fit to the STO data [3] within  $2 \leq T \leq 110$  K yields  $C = (3 \pm 2) 10^6$ ,  $T_S = (17 \pm 1)$  K,  $T_0^Q \approx 0$ , and the highly non-classic exponent  $\gamma = 1.7 \pm 0.2$ . Interestingly, a very similar value,  $\gamma \approx 2$ , was recently obtained on pure STO from a conventional power-law fit for  $4 \leq T \leq 50$  K [4], where saturation effects deviated below  $\approx 4$  K. While our approach matches with this extreme quantum regime without any extra conditions, the  $\Phi^4$  model of [4] requires corrections due to long-range dipolar interactions and coupling of the electric polarization field to acoustic phonons.

## 2. Routes of $\text{SrTiO}_3$ Toward Ferroelectricity and Other Collective States

Overcoming quantum paraelectricity and reaching stable long-range ordered states by proper treatments has remained a major challenge for ongoing research on STO.

- (i) In 1976, Uwe and Sakudo [5] succeeded in stabilizing uniaxial ferroelectricity in STO at liquid He temperature by intraplanar symmetry breaking with uniaxial stress perpendicularly to the  $c$  axis,  $\sigma_{110}$ . This was the first experience to overcome quantum paraelectricity of STO by an external perturbation.
- (ii) About 20 years later, in 1999, Itoh et al. [6] discovered a very efficient internal perturbation via isotopic exchange of  $^{16}\text{O}$  by  $^{18}\text{O}$  in order to establish the FE state at  $T_0 \approx 25\text{--}50$  K.
- (iii) Again, 20 years later, in 2019, Nova et al. [7] realized transient FE in STO being metastable up to  $T > 290$  K under optical strain due to intense femtosecond laser pulses, while Li et al. [8] recorded similar events after photoexcitation of quantum paraelectric STO with THz laser pulses in resonance with the FE soft mode at  $T < 36$  K.
- (iv) Metallic behavior of  $n$ -type STO has been achieved by substituting transition-metal dopants, e.g.,  $\text{La}^{3+}$  for  $\text{Sr}^{2+}$  [9],  $\text{Nb}^{5+}$  for  $\text{Ti}^{4+}$ , or by reducing pure STO into  $\text{SrTiO}_{3-\delta}$ ,  $0 < \delta < 1$ , where each oxygen vacancy generates two “doped” electrons [10]. The insulator-to-metal transformation occurs at a relatively low critical electron density  $n \approx 10^{18} \text{ cm}^{-3}$  [11], i.e., two orders of magnitude less than

in the analogous case of barium titanate [12]. Here the word “metal” is not used in its common material meaning but merely stands for featuring metallic electronic conduction. A combined method of substitution and reduction was utilized in the case of Cr-doped STO [11]. A significant spatial correlation between oxygen vacancies and Cr<sup>3+</sup> ions in bulk was established in thermally reduced Cr-doped STO. In the presence of electron donors, the Cr atoms change their valence from 4+ to 3+. Consequently, this reduction drives a symmetry change of the crystal field experienced by the Cr ions from cubic to axial [11], which may be controlled by means of thermal annealing and/or doping with electron donors. This capability of controlling oxygen vacancies or transition-metal dopants has been essential for the development of semiconducting electronic devices [13].

- (v) Theoretical predictions of superconductivity in degenerate semiconductors motivated research on reduced *n*-type STO, which revealed the critical temperature  $T_c \approx 0.28$  K as early as 1964 [14]. However, 32 years later, perovskite-like cuprates were to open the door to modern high- $T_c$  superconductivity with  $T_c \approx 30$  K [15] and to the physics Nobel Prize [16]. On the other hand, gated *n*-type STO has reached at most only  $T_c \approx 0.6$  K [17].

Meanwhile numerous other processes have made STO a nearly inexhaustible source of activating novel solid state phenomena that suggest future applications. This has remained an attractive research goal even more than 60 years after the pioneering experiments. Extending the initial idea of breaking the local symmetry by stress [5], Bednorz and Müller [2] introduced an *A*-site doping route by random replacement of Sr<sup>2+</sup> ions with smaller Ca<sup>2+</sup> ions in single crystals of Sr<sub>1-x</sub>Ca<sub>x</sub>TiO<sub>3</sub> (SCT). The local decrease of volume creates random strain (“negative stress field”), which has an enormous effect on the dielectric response for doping levels  $0.002 \leq x \leq 0.12$ , as shown in Figure 1 (curves 2–11). Sharp peaks occur at finite temperatures,  $10 < T_m < 40$  K, which clearly hint at polar phase transitions (PTs). Their easy axes are actually lying along  $[110]$  and  $[1\bar{1}0]$  within the basal *xy*-plane and yield, e.g.,  $\epsilon_{max}^{<110>} = 1.1 \cdot 10^5$  for  $x = 0.0107$  [2]. Discussion within a random-field concept of PTs reveals *xy*-type quantum ferroelectricity above  $x_c = 0.0018$  along the *a* axes of the paraelectric parent phase and a PT into a random phase above  $x_r \approx 0.016$  (Figure 1). Quantum corrections to the temperature (see Equation (1)) are essential to describe the critical behavior.

In order to understand more details, some of us measured the optical linear birefringence (LB),  $\Delta n_{ac} = n_c - n_a$ , where  $n_c$  and  $n_a$  are the principal refractive indices at light wavelength  $\lambda = 589.3$  nm, being linearly polarized along the *c* and *a* axes of the SCT crystal, respectively, as functions of temperature, *T* [18]. It is well-known that the LB is sensitive to both the axial rotation of the TiO<sub>6</sub> octahedra,  $\langle \Delta \Phi^2 \rangle$ , below the antiferrodistortive phase transition temperature  $T_a = 105$  K (for  $x = 0$ ), and to the FE short-range order parameter,  $\langle P_x^2 \rangle$ , where  $x \parallel \langle 110 \rangle_c$  (Figure 1). Indeed, non-zero LB arises in pure STO at the transition temperature  $T_a = 105$  K and at 115, 140, and 255 K (arrows) for  $x = 0.002, 0.0107, \text{ and } 0.058$ , respectively, as shown in Figure 2. Additional FE anomalies,  $\delta(\Delta n_{ac})$ , are superposed at low *T*. Being non-morphic, they start smoothly with fluctuation tails and bend over into steeply rising long-range order parts below inflection points  $T_1 \approx 15, 28, \text{ and } 50$  K, respectively (arrows). These temperatures systematically exceed the  $\epsilon'$  vs. *T* peak temperatures,  $T_m = 14, 26, \text{ and } 35$  K, respectively (Figure 1), where discontinuities of  $d(\Delta n_{ac})/dT$  would be expected in case of PTs into long-range order. Absence of anomalies of this type and increasing differences,  $T_1 - T_m$ , at increasing *x* hint at continuously growing smearing of the PTs. Simultaneously, as  $T \rightarrow 0$ , the polarization was calculated by use of the ordinary refractive index  $n_o = 2.41$  and the electro-optic coefficient difference  $g_{11} - g_{31} = 0.14 \text{ m}^4/\text{C}^2$  as  $\langle P_x^2 \rangle^{1/2} = \{2\delta(\Delta n_{ac})/[n_o^3(g_{11} - g_{31})]\} = 9.8, 29.4, \text{ and } 42.6 \text{ mC}/\text{m}^2$  for  $x = 0.002, 0.0107, \text{ and } 0.058$ , respectively [18]. Since  $\langle P_x^2 \rangle^{1/2}$  varies less than proportionally with *x*, comparatively incomplete FE order is observed. Further, the low-*T* polarization saturates, albeit slowly, at increasing electric field, *E*. This strongly hints at random-field induced nanodomains, whose average size increases with an applied ordering field. The increase of the average order parameter gives credit for disappearing domain walls as known from the domain-state FE  $\text{K}_{0.974}\text{Li}_{0.026}\text{TaO}_3$  [19].

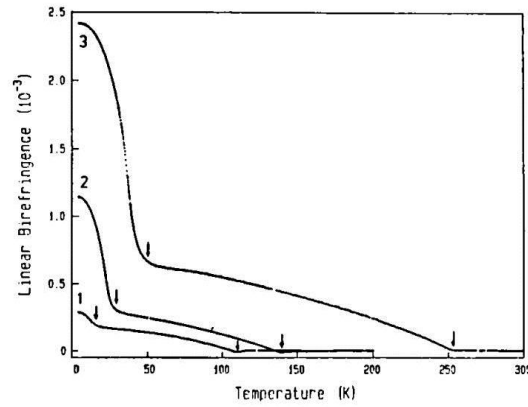


**Figure 2.** Linear birefringence  $\Delta n_{ac}$  vs.  $T$  measured at  $\lambda = 589.3$  nm on crystallographic single domains of  $\text{Sr}_{1-x}\text{Ca}_x\text{TiO}_3$  with  $x = 0.002$  (1), 0.0107 (2), and 0.058 (3), respectively [18].

Further insight into FE SCT is gained from its relaxational behavior. Figure 3 shows the temperature dependence of the real and imaginary parts of the dielectric permittivity of SCT ( $x = 0.002$ ),  $\epsilon'$ , and  $\epsilon''$  vs.  $T$ , at frequencies  $10^3 \leq f \leq 10^4$  Hz [20]. In view of the rounded peaks of  $\epsilon'(T)$ , a polydomain state of this FE is conjectured. This has first been interpreted within the concept of “dynamical heterogeneity” [21], which assumes a manifold of mesoscopic “dynamically correlated domains”, relaxing exponentially with uniform single relaxation times. Their superposition defines the observed polydispersivity of the sample. It represents aggregates of polar clusters surrounding the quenched off-center  $\text{Ca}^{2+}$  dopant dipoles.

It is noticed that  $\epsilon'$  vs.  $T$  peaks at a “glass temperature”,  $T_g \approx 3.8$  K (Figure 3, arrow), in the quasi-static limit,  $f = 1$  mHz, although at first glance, no glassy criticality as in spin glass is expected. However, in view of recently ascertained magnetic superspin glasses (SSG) of dipolarly coupled magnetic nanoparticles at low concentration [22], a related electric superdipolar glass (SDG) has become envisaged. It should behave like a relaxor ferroelectric [23] in terms of a superglassy critical power law behavior of the  $\epsilon''(f)$  vs.  $T$  peak position  $T_m$ .

$$f(T_m) \propto (T_m - T_g^e)^{z\nu}. \quad (2)$$

Evaluation over the whole range of frequencies,  $10^{-3} \leq f \leq 10^4$  Hz, yields the expected dynamic critical exponent  $z\nu \approx 10$  at  $f > 1$  Hz, while systematic deviations occur at lower  $f$  due to the well-known additional tunneling dynamics. Tests on the expected non-ergodicity of the SDG phase at  $T < T_g$  upon zero-field- and field-cooled temperature cycles, respectively (cf. Section 3) are in preparation.

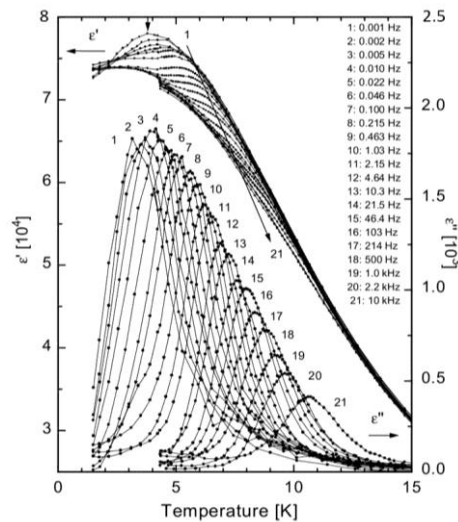


**Figure 3.** Real and imaginary parts of the permittivity,  $\epsilon'$  and  $\epsilon''$  vs.  $T$ , of  $\text{Sr}_{0.998}\text{Ca}_{0.002}\text{TiO}_3$  measured within  $1.5 \leq T \leq 15$  K at frequencies  $10^{-3} \leq f \leq 10^4$  Hz [20].  $T_g \approx 3.8$  K is indicated by an arrow.

At higher concentration of  $\text{Ca}^{2+}$ , the polar nanoregions (PNRs) percolate into an FE groundstate, as proven by first-order Raman scattering at the softening  $F_{1u}$  phonon mode in SCT ( $x = 0.007$ ) at  $T < T_0 = 18$  K [24]. SCT thus succeeds in demonstrating stable ferroelectricity. However, systematic research at increasing Ca content showed that  $T_0$  is limited to  $\approx 35$  K, where the dielectric anomaly becomes increasingly smeared [25]. Better success was achieved by the classic method of stress-induced ferroelectricity in pure STO [5]. To this end Haeni et al. [26] utilized 50 nm thick films of STO, which were epitaxially grown with approximately +1.5% biaxial tensile strain on a (110) $\text{DyScO}_3$  substrate, while  $-0.9\%$  uniform compression due to a  $(\text{LaAlO}_3)_{0.29}(\text{SrAl}_{0.5}\text{Ta}_{0.5}\text{O}_3)_{0.71}$  (LSAT) substrate was barely active in this respect (Figure 4). The high permittivity in the films on  $\text{DyScO}_3$ ,  $\epsilon'$  up to 7000 at 10 GHz and room temperature, as well as its sharp dependence on an electric field is promising for device applications [4,26]. The observation of stress-induced ferroelectricity in STO films has confirmed theoretical predictions of Pertsev et al. [27]. While substrate-induced tensile strain in epitaxial STO films via lattice parameter mismatch favors in-plane FE, compressive strain provides out-of-plane directed ferroelectricity [27]. This was observed by Fuchs et al. [28] at an STO film epitaxially grown on an STO substrate coated by compressive  $\text{YBa}_2\text{Cu}_3\text{O}_7$ .

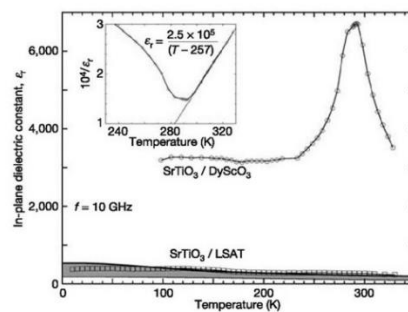


**Figure 4.** In-plane permittivity  $\epsilon'$  vs.  $T$  of a strained 50 nm epitaxial  $\text{STO}/(110)\text{DyScO}_3$  film at  $f = 10$  GHz as compared to a compressed  $\text{STO}/\text{LSAT}$  film. The inset shows a Curie–Weiss fit to  $(\epsilon')^{-1}$  with  $T_0 \approx 260$  K [26].

Another realization of room temperature ferroelectricity in STO confirms theoretical predictions of proximity effects at interfaces of metals to oxides containing PNRs such as, for example, STO [29]. Lee et al. [30] reported emergence of room temperature ferroelectricity at reduced dimensions, thus refuting a long-standing contradicting notion. Piezoelectric force microscopy (PFM) was able to evidence room-temperature ferroelectricity in strain-free epitaxial films with 24 unit-cell-thickness of otherwise non-ferroelectric STO (Figure 5). Following arguments from defect engineering in SCT, the authors claimed that electrically induced alignments of PNRs at Sr deficiency related defects are responsible for the appearance of a stable net of ferroelectric polarization in these films. This insight might be useful for the development of low- $D$  materials of emerging nanoelectronic devices.

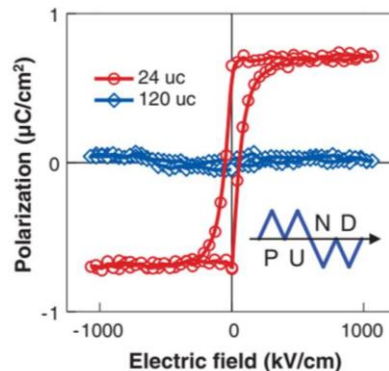


**Figure 5.** Polarization hysteresis of 24 and 120 unit-cell-thick STO films at room temperature, measured by using the double-wave PUND technique with a triangular  $ac$  electric field of 10 kHz (see schematic inset). The hysteresis component is obtained by subtracting the non-hysteretic (up (U) and down (D)) from the total (positive (P) and negative (N)) polarization runs [30].

To systematically control ferroelectricity in thin films of STO at room temperature, Kang et al. [31] selectively engineered elemental vacancies by pulsed laser epitaxy (PLE).  $\text{Sr}^{2+}$  vacancies play an essential role in inducing the cubic-to-tetragonal transition, since they break the inversion symmetry, which is necessary for switchable electric polarization. The tetragonality turns out to increase with increasing vacancy density, thus strengthening the ferroelectricity, as shown in Figure 6a. This research has optimized tetragonality-induced ferroelectricity in STO with reliable growth control of the behavior. PFM yields stable hysteresis loops at room temperature, as shown in Figure 6b, where low and high laser fluences during PLE clearly demonstrate their key role in creating FE polarization. Similar propositions were made by the Barthélémey–Bibes group, which invoked both an electric field-switchable two-dimensional electron gas emerging in ferroelectric SCT films [32] and the non-volatile electric control of spin–charge conversion in an STO Rashba system [33].

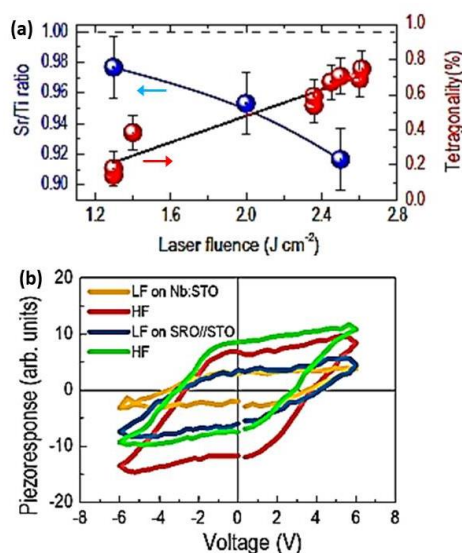


**Figure 6.** (a) Sr/Ti elemental concentration ratio (blue circles) and tetragonality measured at room temperature (red circles) plotted as functions of the laser fluence during pulsed laser epitaxy (PLE). (b) Ferroelectric hysteresis loops recorded by piezoelectric force microscopy (PFM) at 5-nm-thick  $\text{SrTiO}_3$  films grown with low and high laser fluences (LF and HF, respectively; see (a)) on different bottom electrodes ( $\text{STO:Nb}$  and  $\text{SrRuO}_3/\text{STO}$ ) [33].

Only recently has another insight into the ferroelectric state of compressively strained STO become available from high-angle annular dark-field imaging in scanning transmission electron microscopy. Salmani–Rezaie et al. [34] observed local polar regions in the room-temperature paraelectric phase of (001)-strained STO films, which were grown on (001) faces of LSAT and underwent an FE transition at low T. This unexpected feature was explained by a locally dipolar-ordered, but globally random phase of displaced  $\text{Ti}^{4+}$  columns, which underwent a disorder–order transition on cooling.

This Section started with different methods to establish long-range order, such as ferroelectricity (FE), metallicity (MT), or superconductivity (SC) in suitably modified STO [2,9,14]. Lately, more demanding procedures have become successful to stabilize the co-existence of apparently contradictory properties, e.g., FE-SC and FE-MT, which appear self-excluding at first glance. In this context, obscure terms such as, for example, “polar metal” and “metallic ferroelectric” or “ferroelectric metal” have been used interchangeably by the research community. Only recently have subtle distinctions of these variants with respect to their electric field switchability been clarified [12], although this topic still remains under debate.

Rischau et al. [35] showed that SC can coexist with an FE-like instability in oxygen-reduced (“*n*-doped”)  $\text{Sr}_{1-x}\text{Ca}_x\text{TiO}_{3-\delta}$  ( $0.002 < x < 0.009$ ,  $0 < \delta < 0.001$ ), where both long-range orders are intimately linked. The FE transition of insulating SCT was found to survive in this reduced modification. Owing to its metallic conductivity, the latter does not show a bulk reversible electric polarization and hence

cannot be a true ferroelectric. However, it shows anomalies in various physical properties at the Curie temperature of the insulator, e.g., Raman scattering evidences that the hardening of the FE soft mode in the dilute metal is identical with what is seen in the insulator. The anomaly in resistivity was found to terminate at a threshold carrier density ( $n^*$ ), near to which the SC transition temperature is enhanced [35]. This evidences the link between SC pairing and FE dipolar ordering, a subject of current attention [36].

Moreover, it is widely accepted that the low- $T$  phase of STO lies in the vicinity of a quantum critical point, where different phases (i.e., paraelectric, antiferrodistortive, FE, MT, and SC) with similar energies compete, while weak residual interactions may stabilize one or several of these states [37–39]. The coexistence of MT and FE states in STO has been addressed under the keyword charge transport in a polar metal by Wang et al. [40], who studied the low- $T$  electrical resistivity in several  $\text{Sr}_{1-x}\text{Ca}_x\text{TiO}_{3-\delta}$  single-crystals at  $\delta > 0$  within  $0.002 < x < 0.01$  (Figure 7). Since both MT and FE are dilute, the distance between mobile MT electrons and fixed FE dipoles can be separately tuned but kept much longer than the interatomic distance. This opens the chance of activating a Ruderman–Kittel–Kasuya–Yosida-like interaction [41] of carriers with local electric moments, which was originally proposed by Glinchuk and Kondakova [42]. They introduced this indirect interaction of FE off-center ions with conduction electrons in order to explain high FE transition temperatures in certain narrow-gap semiconductors with high conductivity, such as  $\text{Pb}_{1-x}\text{Ge}_x\text{Te}$ . In agreement with this theory, it is expected that the threshold concentration of carriers,  $n^*$ , is proportional to  $x$ , which indicates that it occurs at a fixed ratio between inter-carrier and inter-dipole distances.

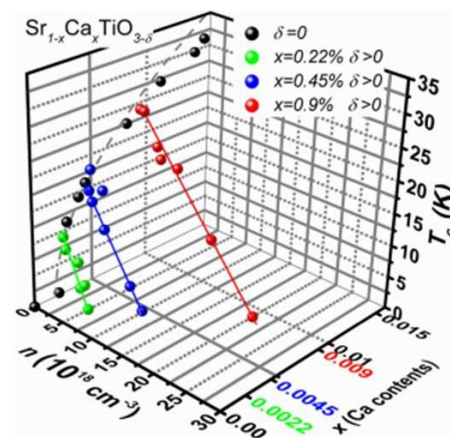


**Figure 7.** Ferroelectric (FE) phase transition temperatures  $T_c$  in insulating  $\text{Sr}_{1-x}\text{Ca}_x\text{TiO}_3$  as functions of  $x$  (black balls [2]) and in metallic  $\text{Sr}_{1-x}\text{Ca}_x\text{TiO}_{3-\delta}$  ( $\delta > 0$ ) as functions of charge carrier density  $n$  and  $x = 0.0022, 0.0045$  and  $0.009$  (green, blue, and red balls, respectively [40]).

Tomioka et al. [17] finally demonstrated the simultaneous occurrence of three states, FE, MT, and SC, by independently controlling two concentrations of electron-doped  $\text{Sr}_{1-x}\text{La}_x\text{Ti}(\text{}^{16}\text{O}_{1-z}\text{}^{18}\text{O}_z)_3$  single crystals. They precisely controlled the “dome-like” SC characteristic by  $n$  doping via the  $\text{La}^{3+}$  content, while independently enhancing  $T_c$  by substitution of  $^{18}\text{O}^{2-}$  ions for  $^{16}\text{O}^{2-}$ . At an electron concentration of  $n \approx 5 \times 10^{19} \text{ cm}^{-3}$ , they found the apex of the SC dome at  $T_c \approx 0.44 \text{ K}$ , where they subsequently shifted its height to a record-high  $T_c \approx 0.6 \text{ K}$  by adjusting  $z(^{18}\text{O})$ .

Being arbitrarily close to the quantum critical point of non-centrosymmetric SC, experiments have thus come into reach to probe mixed-parity pairing mechanisms with topological aspects to their SC states, such as extremely large and highly anisotropic upper critical fields and topologically protected spin currents. A decisive step toward this aim was done by Schumann et al. [43] using  $\text{La}^{3+}$  or  $\text{Sm}^{3+}$   $n$ -doped STO films on (001)-strained LSAT substrates. Being in their polar phase, they reveal enhanced superconducting  $T_c$ , while some of them show signatures of an unusual SC state, where the in-plane critical field is higher than both the paramagnetic and orbital pair breaking limits. Moreover, nonreciprocal transport is observed, which reflects the ratio of odd versus even pairing interactions. A similar highlight was observed in a gate-induced 2D SC of interfacial STO [44]. Due to its Rashba-

type spin orbit interaction, it reveals nonreciprocal transport, where the inequivalent rightward and leftward currents reflect simultaneous spatial inversion and time-reversal symmetry breaking—an exciting prospect of forthcoming research on STO.

### 3. The Magnetoelectric Multiglass (Sr,Mn)TiO<sub>3</sub>

The nature of glassy states in disordered materials has long been controversially discussed. In the magnetic community, generic spin glasses have long been accepted to undergo phase transitions at a static glass temperature  $T_g$ , where they exhibit criticality and originate well-defined order parameters [45]. In addition, disordered polar systems are expected to transit into generic “dipolar” or “orientational glass” states [46], which fulfil similar criteria as spin glasses. Hence, it appears quite natural to introduce the term “multiglass” for a new kind of multiferroic material revealing both polar and spin glass properties, which were discovered by some of us in the ceramic solid solution  $\text{Sr}_{0.98}\text{Mn}_{0.02}\text{TiO}_3$  [47]. By various experimental methods [48–50] it has been ascertained that the  $\text{Mn}^{2+}$  ions are randomly substituting  $\text{Sr}^{2+}$  ions on A-sites in quantum paraelectric STO (Figure 8a), where they become off-centered due to their small ionic size and undergo covalent bonding with one of the twelve nearest neighboring  $\text{O}^{2-}$  ions. These elementary dipoles readily form polar nanoclusters with frustrated dipolar interactions, as illustrated in Figure 8b. It depicts the local cluster formation of  $\text{Mn}^{2+}$  ions with antiparallel electric dipole moments and antiferromagnetically correlated spins.

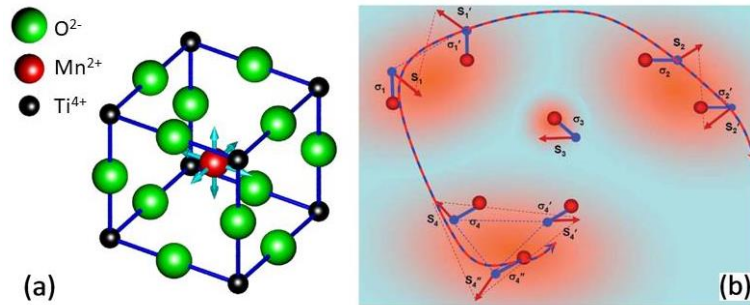


**Figure 8.** (a) A site substituted  $\text{Mn}^{2+}$  ion in its cage of 12 nearest neighboring oxygen ions in the  $\text{ABO}_3$  lattice of STO going off-center along  $\langle 100 \rangle$  [46]. (b) Schematic structure of  $\text{SrTiO}_3:\text{Mn}^{2+}$  highlighting a percolating multiglass path of randomly distributed  $\text{Mn}^{2+}$  ions (red–blue broken line) carrying dipole moments  $\sigma_j$  (blue lines) and spins  $S_j$  (red arrows) with electric dipolar and antiferromagnetic correlations, respectively, within polar STO clusters (red “clouds”) [51].

The dipolar glass formation can easily be judged from the asymptotic shift of the dynamic dielectric susceptibility peak,  $T_m(f)$ , at frequencies within the range  $10^{-1} \leq f \leq 10^6$  Hz in Figure 9a. It obeys glassy critical behavior according to Equation (2), where  $z\nu = 8.5$  is the dynamic critical exponent and  $T_g^e \approx 38$  K the electric glass temperature [51]. On the other hand, frustrated and random  $\text{Mn}^{2+}-\text{O}^{2-}-\text{Mn}^{2+}$  superexchange is at the origin of spin glass formation below the magnetic glass temperature  $T_g^m \approx 34$  K. This temperature marks the confluence of three characteristic magnetization curves recorded in  $\mu_0 H = 10$  mT after zero-field cooling (ZFC) to  $T = 5$  K upon field heating ( $m^{\text{ZFC}}$ ), upon subsequent field cooling ( $m^{\text{FC}}$ ), and thereafter the thermoremanence ( $m^{\text{TRM}}$ ) upon zero-field heating (ZFH) as shown in Figure 9c. It should be noticed that both glassy states have unanimously been confirmed by clear-cut individual aging, rejuvenation, and memory effects in their respective  $dc$  susceptibilities [51]. “Holes” burnt into the electric and magnetic susceptibilities by waiting in zero external field for 10.5 h at 32.8 K and for 2.8 h at 33 K, respectively, and subsequent heating with weak electric or magnetic probing fields are shown in Figure 9b,d, respectively. They corroborate the glassy ground states of both polar and magnetic subsystems and their compatibility with spin glass theory [45]. Observation of the biquadratic ME interaction in the free energy [47],

$$F(E, H) = F_0 - (\delta/2)E_i E_j H_k H_l (i, j, k, l = 1, 2, 3), \quad (3)$$

is compatible with the low symmetry of the compound and is thought to crucially reinforce the spin glass ordering, as schematically depicted in Figure 8b [51]. Similarly to the dielectric anomaly [52], the magnetic anomaly has been found to depend not only on the frequency, but crucially also on the Mn content, confirming its intrinsic origin [53]. Furthermore, apart from ceramics, both glassy states have also been detected in equivalent thin films [54].

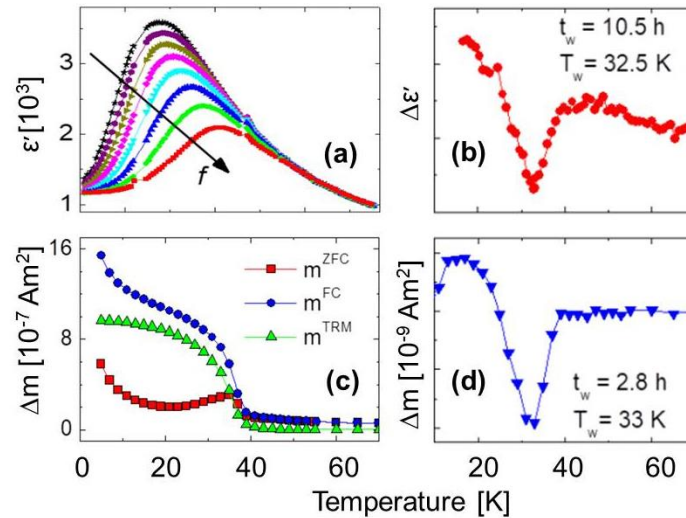


**Figure 9.** (a) Dielectric susceptibility  $\epsilon'(T)$  of  $\text{Sr}_{0.98}\text{Mn}_{0.02}\text{TiO}_3$  ceramics recorded at frequencies  $10^{-1} \leq f \leq 10^6$  Hz and (c) magnetization measured in  $B = 10$  mT on field heating after ZFC ( $m^{\text{ZFC}}$ ), on FC ( $m^{\text{FC}}$ ), and on ZFH after FC ( $m^{\text{TRM}}$ ). Holes  $\Delta\epsilon(T)$  and  $\Delta m(T)$  burnt in zero fields at  $T_{\text{wait}} = 32.5$  K for 10.5 h (b) and  $T_{\text{wait}} = 33$  K for 2.8 h (d) confirm memory and rejuvenation of both electric and magnetic glassy subsystems [47].

Starting from a mean-field ansatz within the framework of a transverse Ising model [51], the complete theory of the ME multiglass is still under debate. In particular, the final steps for establishing the spin glass are missing. It is thought to emerge from multipolar interaction of spin clusters (Figure 8b) and probably comes close to the formation of a superspin glass as in systems of magnetic nanoparticles [22]. Since these probably consist of antiferromagnetic  $\text{MnTiO}_3$  and carry merely surface magnetization [55], special care has to be taken.

In search of other ME multiglasses, we successfully examined also  $\text{Mn}^{2+}$  doped  $\text{KTaO}_3$ , which in the undoped case is a quantum paraelectric like STO, but nevertheless has slightly different properties on doping [56]. Other research groups have made similar experiments, and all of them reported considerable complexity [57–60]. Moreover, various other ME multiglasses have also been observed in disordered solid solutions such as  $\text{CuFe}_{0.5}\text{V}_{0.5}\text{O}_2$  [61],  $\text{La}_2\text{NiMnO}_6$  [62],  $\text{Fe}_2\text{TiO}_5$  [63], and  $(\text{Ba}_3\text{NbFe}_3\text{Si}_2\text{O}_{14})\text{:Sr}$  [64].

#### 4. Conclusions

STO still enjoys vivid interest in research and technological development. Having overcome the low-T bottleneck by advanced nanotechnologies, STO belongs to the most promising nanoelectronic materials. Unusual properties around the quantum critical point such as the co-existence of regular and superconductivity with ferroelectricity are still the focus of attention. On the other hand, the novel disordered phases of a superglass in  $\text{Sr}_{0.998}\text{Ca}_{0.002}\text{TiO}_3$  and a multiglass in  $\text{Sr}_{0.98}\text{Mn}_{0.02}\text{TiO}_3$  also still require dedicated activity.

**Author Contributions:** Conceptualization, W.K.; writing—original draft preparation, W.K.; writing—review and editing, W.K., J.D., A.T. and P.M.V. All authors have read and agreed to the published version of the manuscript.

**Funding:** This research received no external funding.

**Acknowledgments:** We are grateful to K.A. Müller and J.G. Bednorz for providing their outstanding single crystal samples of SCT and cooperating within common publications. In addition, we acknowledge valuable cooperation with A. Albertini, S. Bedanta, U. Bianchi, P. Borisov, A. Hochstrat, S. Miga, F.J. Schäfer, and V.V. Shvartsman.

**Conflicts of Interest:** The authors declare no conflict of interest.

## Glossary

FC = field cooling, FE = ferroelectric or ferroelectricity, FH = field heating, LB = linear birefringence, LSAT =  $(\text{LaAlO}_3)_{0.29}(\text{SrAl}_{0.5}\text{Ta}_{0.5}\text{O}_3)_{0.71}$ , MT = metallic or metallicity, PLE = pulsed laser epitaxy, PNR = polar nanoregion, PT = phase transition, SC = superconductive or superconductivity, SCT =  $\text{Sr}_{1-x}\text{Ca}_x\text{TiO}_3$ , STO =  $\text{SrTiO}_3$ , TRM = thermoremanence, ZFC = zero-field cooling, ZFH = zero-field heating.

## References

- Müller, K.A.; Burkard, H.  $\text{SrTiO}_3$ : An intrinsic quantum paraelectric below 4 K. *Phys. Rev. B* **1979**, *19*, 3593–3602.
- Bednorz, J.G.; Müller, K.A.  $\text{Sr}_{1-x}\text{Ca}_x\text{TiO}_3$ : An XY quantum ferroelectric with transition to randomness. *Phys. Rev. Lett.* **1984**, *52*, 2289–2293.
- Dec, J.; Kleemann, W. From Barrett to generalized quantum Curie-Weiss law. *Solid State Commun.* **1998**, *106*, 695–699.
- Rowley, S.E.; Spalek, L.J.; Smith, R.P.; Dean, M.P.M.; Itoh, M.; Scott, J.F.; Lonzarich, G.G.; Saxena, S.S. Ferroelectric quantum criticality. *Nat. Phys.* **2014**, *10*, 367–372.
- Uwe, H.; Sakudo, T. Stress-induced Ferroelectricity and soft phonon modes in  $\text{SrTiO}_3$ . *Phys. Rev. B* **1976**, *13*, 271–286.
- Itoh, M.; Wang, R.; Inaguma, Y.; Yamaguchi, T.; Shan, Y.-J.; Nakamura, T. Ferroelectricity induced by oxygen isotope exchange in strontium titanate perovskite. *Phys. Rev. Lett.* **1999**, *82*, 3540–3543.
- Nova, T.F.; Disa, A.S.; Fechner, M.; Cavalleri, A. Metastable ferroelectricity in optically strained  $\text{SrTiO}_3$ . *Science* **2019**, *364*, 1075–1079.
- Li, X.; Qiu, T.; Zhang, J.; Baldini, E.; Lu, J.; Rappe, A.M.; Nelson, K.A. Terahertz field-induced ferroelectricity in quantum paraelectric  $\text{SrTiO}_3$ . *Science* **2019**, *364*, 1079–1082.
- Tokura, Y.; Taguchi, Y.; Okada, Y.; Fujishima, Y.; Arima, T.; Kumagai, K.; Iye, Y. Filling dependence of electronic properties on the verge of metal-Mott-insulator. *Phys. Rev. Lett.* **1993**, *70*, 2126–2129.
- Spinelli, A.; Torija, M.A.; Liu, C.; Jan, C.; Leighton, C. Electronic transport in doped  $\text{SrTiO}_3$ : Conduction and potential applications. *Phys. Rev. B* **2010**, *81*, 155110.
- La Mattina, F.; Bednorz, J.G.; Alvarado, S.F.; Shengelaya, A.; Müller, K.A.; Keller, H. Controlled oxygen vacancies and space correlation with  $\text{Cr}^{3+}$  in  $\text{SrTiO}_3$ . *Phys. Rev. B* **2009**, *80*, 075122.
- Zhou, W.X.; Ariando, A. Review on Ferroelectric/polar metals. *Jpn. J. Appl. Phys.* **2020**, *59*, S10802.
- Alvarado, S.P.; La Mattina, P.; Bednorz, J.G. Electroluminescence in  $\text{SrTiO}_3$ : Cr single-crystal nonvolatile memory cells. *Appl. Phys. A* **2007**, *89*, 85–89.
- Schooley, J.F.; Hosler, W.R.; Cohen, M.L. Superconductivity in semiconducting  $\text{SrTiO}_3$ . *Phys. Rev. Lett.* **1964**, *12*, 474–475.
- Bednorz, J.G.; Müller, K.A. Possible high- $T_c$  superconductivity in the Ba-La-Cu-O system. *Z. Phys. B Cond. Matter* **1986**, *64*, 189–193.
- Bednorz, J.G.; Müller, K.A. Perovskite-type oxides—The new approach to high- $T_c$  superconductivity. *Nobel Lect. Dec.* **1987**. Available online: <https://www.nobelprize.org/uploads/2018/06/bednorz-muller-lecture.pdf> (accessed on 1 April 2020).
- Tomioka, Y.; Shirakawa, N.; Shibuya, K.; Inoue, I.H. Enhanced superconductivity close to a nonmagnetic quantum critical point in electron-doped strontium titanate. *Nat. Commun.* **2019**, *10*, 738.
- Kleemann, W.; Schäfer, F.J.; Müller, K.A.; Bednorz, J.G. Domain state properties of the random-field  $xy$ -model system  $\text{Sr}_{1-x}\text{Ca}_x\text{TiO}_3$ . *Ferroelectrics* **1988**, *80*, 297–300.
- Kleemann, W.; Kütz, S.; Rytz, D. Cluster glass and domain state properties of  $\text{K}_{1-x}\text{Li}_x\text{TaO}_3$ . *Europhys. Lett.* **1987**, *4*, 239–245.
- Kleemann, W.; Albertini, A.; Chamberlin, R.V.; Bednorz, J.G. Relaxational dynamics of polar nano-domains in  $\text{Sr}_{1-x}\text{Ca}_x\text{TiO}_3$ ,  $x = 0.002$ . *Europhys. Lett.* **1997**, *37*, 145–150.
- Chamberlin, R.V.; Haines, D.N. Percolation model for relaxation in random systems. *Phys. Rev. Lett.* **1990**, *65*, 2197–2200.

22. Bedanta, S.; Kleemann, W. Supermagnetism. *J. Phys. D Appl. Phys.* **2009**, *42*, 013001.
23. Kleemann, W. Relaxor ferroelectrics: Cluster glass ground state via random fields and random bonds. *Phys. Status Solidi B* **2014**, *251*, 1993–2002.
24. Bianchi, U.; Kleemann, W.; Bednorz, J.G. Raman scattering of ferroelectric  $\text{Sr}_{1-x}\text{Ca}_x\text{TiO}_3$ ,  $x = 0.007$ . *J. Phys. Condens. Matter* **1994**, *6*, 1229–1238.
25. Carpenter, M.A.; Howard, C.J.; Knight, K.S.; Zhang, Z. Structural relationships and a phase diagram for (Ca, Sr)TiO<sub>3</sub> perovskites. *J. Phys. Condens. Matter* **2006**, *18*, 10725–10749.
26. Haeni, J.H.; Irvin, P.; Chang, W.; Uecker, R.; Reiche, P.; Li, Y.L.; Choudhury, S.; Tian, W.; Hawley, M.E.; Craigo, B.; et al. Room-temperature ferroelectricity in strained SrTiO<sub>3</sub>. *Nature* **2004**, *430*, 758–761.
27. Pertsev, N.A.; Tagantsev, A.K.; Setter, N. Phase transitions and strain-induced ferroelectricity in SrTiO<sub>3</sub> epitaxial thin films. *Phys. Rev. B* **2000**, *61*, R825–R829.
28. Fuchs, D.; Schneider, C.W.; Schneider, R.; Rietschel, H. High dielectric constant and tunability of epitaxial thin film capacitors. *J. Appl. Phys.* **1999**, *85*, 7363–7369.
29. Stengel, M.; Spaldin, N.A. Origin of the dielectric dead layer in nanoscale capacitors. *Nature* **2006**, *443*, 679–682.
30. Lee, D.; Lu, H.; Gu, Y.; Choi, S.-Y.; Li, S.-D.; Ryu, S.; Paudel, T.R.; Song, K.; Mikheev, E.; Lee, S.; et al. Emergence of room-temperature ferroelectricity at reduced dimensions. *Science* **2015**, *349*, 1314–1317.
31. Kang, K.T.; Seo, H.I.; Kwon, O.; Lee, K.; Bae, J.-S.; Chu, M.-W.; Chae, S.C.; Kim, Y.; Choi, W.S. Ferroelectricity in SrTiO<sub>3</sub> epitaxial thin films via Sr-vacancy-induced tetragonality. *Appl. Surf. Sci.* **2020**, *499*, 143930.
32. Bréhin, J.; Trier, F.; Vicente-Arche, L.M.; Hemme, P.; Noël, P.; Cosset-Chéneau, M.; Attané, J.-P.; Vila, L.; Sander, A.; Gallais, Y.; et al. Switchable two-dimensional electron gas based on ferroelectric Ca: SrTiO<sub>3</sub>. *Phys. Rev. Mater.* **2020**, *4*, 041002.
33. Noël, P.; Trier, F.; Vicente-Arche, L.M.; Bréhin, J.; Vaz, D.C.; Garcia, V.; Fusil, S.; Barthélémy, A.; Vila, L.; Bibes, M.; et al. Non-volatile electric control of spin–charge conversion in a SrTiO<sub>3</sub> Rashba system. *Nature* **2020**, *580*, 483–486.
34. Salmani-Rezaie, S.; Ahadi, K.; Strickland, W.M.; Stemmer, S. Order-disorder ferroelectric transition of strained SrTiO<sub>3</sub>. *Phys. Rev. Lett.* **2020**, *125*, 087601.
35. Rischau, C.W.; Lin, X.; Grams, C.P.; Finck, D.; Harms, S.; Engelmayer, J.; Lorenz, T.; Gallais, Y.; Fauqué, B.; Hemberger, J.; Behnia, K. A ferroelectric quantum phase transition inside the superconducting dome of Sr<sub>1-x</sub>Ca<sub>x</sub>TiO<sub>3-δ</sub>. *Nat. Phys.* **2017**, *13*, 643–648.
36. Wölfle, P.; Balatsky, A.V. Superconductivity at low density near a ferroelectric quantum critical point: Doped SrTiO<sub>3</sub>. *Phys. Rev. B* **2018**, *98*, 104505.
37. Takada, Y. Theory of superconductivity in polar semiconductors and its application to *n*-type semiconducting SrTiO<sub>3</sub>. *J. Phys. Soc. Jpn.* **1980**, *49*, 1267–1275.
38. Gabay, M.; Triscone, J.-M. Superconductivity: Ferroelectricity woos pairing. *Nat. Phys.* **2017**, *13*, 624–625.
39. Collignon, C.; Lin, X.; Rischau, C.W.; Fauqué, B.; Behnia, K. Metallicity and superconductivity in doped strontium titanate. *Ann. Rev. Cond. Matt. Phys.* **2019**, *10*, 25–44.
40. Wang, J.L.; Yang, L.W.; Rischau, C.W.; Xu, Z.K.; Ren, Z.; Lorenz, T.; Hemberger, J.; Lin, X.; Behnia, K. Charge transport in a polar metal. *NPJ Quantum Mater.* **2020**, *4*, 61–68.
41. Available online: [https://en.wikipedia.org/wiki/RKKY\\_interaction](https://en.wikipedia.org/wiki/RKKY_interaction) (accessed on 15 April 2020).
42. Glinchuk, M.D.; Kondakova, I.V. Ruderman–Kittel–like interaction of electric dipoles in systems with carriers. *Phys. Stat. Sol.* **1992**, *174*, 193–197.
43. Schumann, T.; Galletti, L.; Jeong, H.; Ahadi, K.; Strickland, W.M.; Salmani-Rezaie, S.; Stemmer, S. Possible signatures of mixed-parity superconductivity in doped polar SrTiO<sub>3</sub> films. *Phys. Rev. B* **2020**, *101*, 100503.
44. Itahashi, Y.M.; Ideue, T.; Saito, Y.; Shimizu, S.; Ouchi, T.; Nojima, T.; Iwasa, Y. Nonreciprocal transport in gate-induced polar superconductor SrTiO<sub>3</sub>. *Sci. Adv.* **2020**, *6*, eaay9120.
45. Binder, K.; Young, A.P. Spin glasses: Experimental facts, theoretical concepts, and open questions. *Rev. Mod. Phys.* **1986**, *58*, 801–976.
46. Binder, K.; Reger, J.D. Theory of orientational glasses: Models, concepts, simulations. *Adv. Phys.* **1992**, *41*, 547–627.
47. Shvartsman, V.V.; Bedanta, S.; Borisov, P.; Kleemann, W.; Tkach, A.; Vilarinho, P.M. (Sr,Mn)TiO<sub>3</sub>: A magnetoelectric multiglass. *Phys. Rev. Lett.* **2008**, *101*, 165704.
48. Laguta, V.V.; Kondakova, I.V.; Bykov, I.P.; Glinchuk, M.D.; Tkach, A.; Vilarinho, P.M.; Jastrabik, L. Electron spin resonance investigation of Mn<sup>2+</sup> ions and their dynamics in Mn-doped SrTiO<sub>3</sub>. *Phys. Rev. B* **2007**, *76*, 054104.

49. Lebedev, A.I.; Sluchinskaya, I.A.; Erko, A.; Kozlovskii, V.F. Direct evidence for off-centering of Mn impurity in SrTiO<sub>3</sub>. *JETP Lett.* **2009**, *89*, 457–460.
50. Levin, I.; Krayzman, V.; Woicik, J.C.; Tkach, A.; Vilarinho, P.M. X-ray absorption fine structure studies of Mn coordination in doped perovskite SrTiO<sub>3</sub>. *Appl. Phys. Lett.* **2010**, *96*, 052904.
51. Kleemann, W.; Bedanta, S.; Borisov, P.; Shvartsman, V.V.; Miga, S.; Dec, J.; Tkach, A.; Vilarinho, P.M. Multiglass order and magnetoelectricity in Mn<sup>2+</sup> doped incipient ferroelectrics. *Eur. Phys. J. B* **2009**, *71*, 407–410.
52. Tkach, A.; Vilarinho, P.M.; Kholkin, A.L. Polar behavior in Mn-doped SrTiO<sub>3</sub> ceramics. *Appl. Phys. Lett.* **2005**, *86*, 172902.
53. Tkach, A.; Vilarinho, P.M.; Kleemann, W.; Shvartsman, V.V.; Borisov, P.; Bedanta, S. Comment on “The origin of magnetism in Mn-doped SrTiO<sub>3</sub>”. *Adv. Funct. Mater.* **2013**, *23*, 2229–2230.
54. Tkach, A.; Okhay, O.; Wu, A.; Vilarinho, P.M.; Bedanta, S.; Shvartsman, V.V.; Borisov, P. Magnetic anomaly and dielectric tunability of (Sr,Mn)TiO<sub>3</sub> thin films. *Ferroelectrics* **2012**, *426*, 274–281.
55. Ribeiro, R.A.P.; Andrés, J.; Longo, F.; Lazaro, S.R. Magnetism and multiferroic properties at MnTiO<sub>3</sub> surfaces: A DFT study. *Appl. Surf. Sci.* **2018**, *452*, 463–472.
56. Shvartsman, V.V.; Bedanta, S.; Borisov, P.; Kleemann, W.; Tkach, A.; Vilarinho, P.M. Spin cluster glass and magnetoelectricity in Mn-doped KTaO<sub>3</sub>. *J. Appl. Phys.* **2010**, *107*, 103926.
57. Valant, M.; Kolodiaznyy, T.; Axelsson, A.-K.; Babu, G.S.; Alford, N.M. Spin ordering in Mn-doped KTaO<sub>3</sub>? *Chem. Mater.* **2010**, *22*, 1952–1954.
58. Venturini, E.L.; Samara, G.A.; Laguta, V.V.; Glinchuk, M.D.; Kondakova, I.V. Dipolar centers in incipient ferroelectrics: Mn and Fe in KTaO<sub>3</sub>. *Phys. Rev. B* **2005**, *71*, 094111–1–8.
59. Golovina, I.S.; Shanina, B.D.; Geifman, I.N.; Andriiko, A.A.; Chernenko, L.V. Specific features of the EPR spectra of KTaO<sub>3</sub>:Mn nanopowders. *Phys. Sol. State* **2012**, *54*, 551–558.
60. Golovina, I.S.; Lemishko, S.V.; Morozovska, A.N. Percolation magnetism in ferroelectric nanoparticles. *Nanoscale Res. Lett.* **2017**, *12*, 382.
61. Singh, K.; Maignan, A.; Simon, C.; Hardy, V.; Pachoud, E.; Martin, C. The spin glass Delafossite CuFe<sub>0.5</sub>V<sub>0.5</sub>O<sub>2</sub>: A dipolar glass? *J. Phys. Condens. Matter* **2011**, *23*, 126005.
62. Choudhury, D.; Mandal, P.; Mathieu, R.; Hazarika, A.; Rajan, S.; Sundaresan, A.; Waghmare, U.V.; Knut, R.; Karis, O.; Nordblad, P.; Sarma, D.D. Near-room-temperature colossal magnetodielectricity and multiglass properties in partially disordered La<sub>2</sub>NiMnO<sub>6</sub>. *Phys. Rev. Lett.* **2012**, *108*, 127201.
63. Sharma, S.; Basu, T.; Shahee, A.; Singh, K.; Lalla, N.P.; Sampathkumaran, E.V. Multiglass properties and magnetoelectric coupling in the uniaxial anisotropic spin-cluster-glass Fe<sub>2</sub>TiO<sub>5</sub>. *Phys. Rev. B* **2014**, *90*, 144426–1–6.
64. Rathore, S.S.; Vitta, S. Effect of divalent Ba cation substitution with Sr on coupled “multiglass” state in the magnetoelectric multiferroic compound Ba<sub>3</sub>NbFe<sub>3</sub>Si<sub>2</sub>O<sub>14</sub>. *Sci. Rep.* **2015**, *5*, 9751.

